


Heat localization through reduced dimensionalityMike Chang,^{1,4} Harrison D. E. Fan,^{1,4} Mokter M. Chowdhury,^{1,4} George A. Sawatzky,^{2,3,4} and Alireza Nojeh^{1,4,*}¹*Department of Electrical and Computer Engineering, University of British Columbia, Vancouver, British Columbia, Canada V6T 1Z4*²*Department of Physics and Astronomy, University of British Columbia, Vancouver, British Columbia, Canada V6T 1Z1*³*Department of Chemistry, University of British Columbia, Vancouver, British Columbia, Canada V6T 1Z1*⁴*Quantum Matter Institute, University of British Columbia, Vancouver, British Columbia, Canada V6T 1Z4* (Received 30 April 2017; revised manuscript received 15 September 2018; published 16 October 2018)

We present a model to show that heat propagation away from a local source depends strongly on dimensionality, leading to dramatic localization in low-dimensional systems. An example of such a system is a carbon nanotube array. We further show that this localization is amplified due to a runaway mechanism if thermal conductivity declines rapidly with temperature. Extremely high temperatures of thousands of kelvins and gradients of hundreds of kelvins per micrometer may thus be obtained in a conductor using a modest local power source such as a laser pointer. This is of fundamental importance for high-efficiency energy conversion through thermoelectric and thermionic mechanisms, as well as various other applications.

DOI: [10.1103/PhysRevB.98.155422](https://doi.org/10.1103/PhysRevB.98.155422)**I. INTRODUCTION**

At finite temperatures, electron transport leads to the transfer of a certain amount of heat as expressed by the Wiedemann-Franz law, although deviations have been observed and attributed to the lack of quasiparticles [1,2]. The other contribution to thermal conductivity is by phonons, making it difficult to maintain a high temperature difference across a device, but this contribution can in principle be made to be small, such as in the phonon-glass structures clathrates [3] and skutterudites [4]. Indeed, limiting heat flow across a conductor or semiconductor is the key challenge in the conversion of thermal to electrical energy. Low-dimensional systems can restrict heat flow due to spatial confinement of phonons and may provide a path to address this long-standing problem [5,6,7]. For example, strongly localized heating and incandescence have been reported in graphene ribbons subject to an electric current [8].

Arrays of vertically aligned multiwalled carbon nanotubes (CNT forests) are quasi one-dimensional (1D) materials with up to macroscopic dimensions, in which nanotubes have long-range alignment [Fig. 1(a)], leading to strongly anisotropic bulk properties. An extreme manifestation of heat confinement has previously been demonstrated experimentally in CNT forests [9]. In this so-called heat trap effect, a beam of light illuminates a spot on the sidewall of the CNT forest; although CNTs are good thermal conductors, surprisingly, the generated heat remains strongly localized not only in the direction perpendicular to the nanotubes but also along the nanotubes. Figure 1(b) shows a photo of a ~ 1.5 -mm-tall CNT forest the sidewall of which is illuminated with an infrared light beam focused to a point with a diameter of approximately 250 μm . The bright region corresponds to the

incandescent glow of the resulting hot spot (the incident beam is not seen in the photo). Using thermographic imaging and hyperspectroscopy, temperature gradients greater than 10 K/ μm have been measured along the nanotubes [10,11]—values that are unprecedented in ordinary isotropic bulk conductors.

This strong confinement allows the structure to reach peak temperatures of >2000 K (leading to thermionic electron emission following the Richardson-Dushman law [12]) with an input optical intensity on the order of only tens of watts per square centimeter, which is three to four orders of magnitude less than the intensities required to heat ordinary conductors to such temperatures. Such facile heating using readily accessible optical powers, together with the fact that the effect is relatively insensitive to the illumination wavelength [13], has been exploited to create simple and compact solar thermionic electron emitters and energy converters [14]. The effect has also enabled the combination of multiphoton photoelectron emission and thermionic electron emission [15]. The physical origins of this strong heat confinement remain unknown. Adding to the puzzle is the fact that, in laser-induced heating of individual CNTs or small bundles, optical intensities thousands of times greater than those used in the heat trap effect have yielded peak temperatures of only a few hundred degrees [16,17]. This suggests that the collective behavior of the large ensemble of the CNTs may play a key role in heat localization as an emergent phenomenon. In the present theoretical/numerical study, we develop a model based on anisotropic heat flow that not only provides an explanation for this effect but may also form the foundation of an approach to confining heat while allowing electricity to flow. The key merit of this approach is that it does not rely on having an inherently low thermal conductivity, thus opening up the possibility of using materials with a variety of electrical properties for energy conversion by shaping them into 1D form.

*Corresponding author: alireza.nojeh@ubc.ca

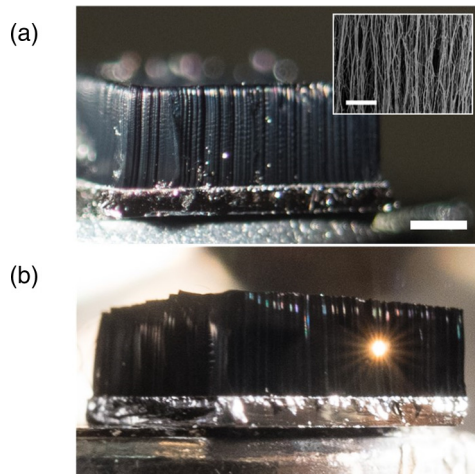


FIG. 1. “Heat trap” on a carbon nanotube forest. (a) Close-up photograph of a ~ 1.5 -mm-tall forest of multiwalled CNTs, showing their vertical alignment. Inset: Scanning electron micrograph of the side of a typical CNT forest. The forest was grown using chemical vapor deposition on a silicon substrate with a thin-film iron catalyst. Scale bars: 1 mm (photo) and 1 μm (inset). (b) Photo of a heat trap spot on the side of the forest under vacuum, upon illumination with an infrared laser beam (wavelength, 1064 nm; approximate spot diameter, 250 μm), which itself is not seen in the photo. Despite high conductivity along the CNTs, the temperature profile exhibits strong confinement, as seen by the localized incandescence from the illuminated hot spot.

II. MODEL

Figure 2 shows a schematic of an illuminated CNT array. Each nanotube dissipates the absorbed optical power through thermal conduction along its axis (dominated by phonons, with possible contributions from other quasiparticles and

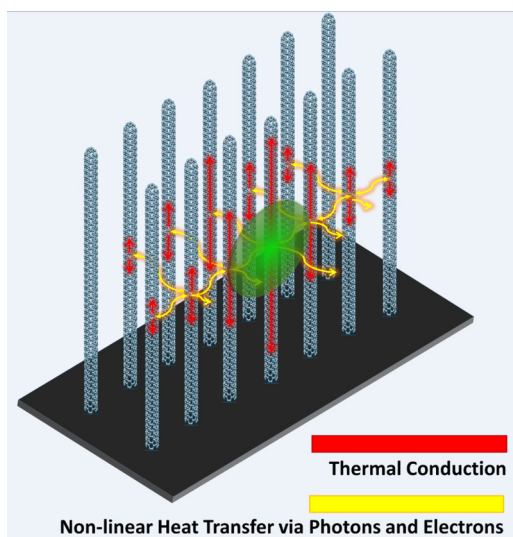


FIG. 2. Dimensionality manifesting as anisotropy. Conceptual representation of optical absorption by an array of aligned carbon nanotubes, showing thermal conduction along each, as well as radiation and electron emission to adjacent nanotubes. The green circle indicates the area to which incident power is delivered.

electrons), as well as reradiation in the form of incandescence (photons) and thermionic emission (electrons). The emitted photons and electrons can in turn be partially reabsorbed by adjacent nanotubes in the forest. The average internanotube spacing is a few tens of nanometers, which is much smaller than the characteristic wavelength of thermal radiation (infrared). The CNTs are thus strongly electromagnetically coupled and the far-field Stefan-Boltzmann law may not be applicable for estimating their radiative energy exchange. The full treatment of this rich and complex electrodynamic problem requires simultaneously solving the optical absorption/reradiation, heat conduction, and electron emission for a large network of coupled CNTs, while taking into account their individual and diverse electronic structures and optical and thermal characteristics. Such an all-encompassing theory is currently out of reach. Fortunately, however, a key property of the CNT forest allows for a much simpler approach. CNT forests have been reported to be extremely dark and behave like a blackbody [18,19]; experiments have revealed that they absorb more than 99.9% of light over a broad spectral range [20]. This may be understood as being the overall result of all the reradiation and reabsorption events by individual nanotubes, effectively leading to the capture of the entire incident optical energy by the forest. The other important consideration is related to thermal conductivity. As expected, thermal conductivity has been predicted and measured to be highly anisotropic in the CNT forest, with the value along the axis of the CNTs being one to two orders of magnitude greater than in the transverse directions [21–23]; similarly, an anisotropy of more than two orders of magnitude has also been reported in silicon nanowire arrays [24]. The question arises as to whether anisotropy persists at very high temperatures, where internanotube radiative coupling, which does not depend on physical contact and phonon flow, may transfer significant amounts of heat in the transverse directions. However, measurements of the temperature profile at high temperatures have shown significantly tighter confinement in the transverse direction than along the nanotubes [10,11], demonstrating that anisotropy persists.

In the context of our model, the above observations allow us to treat the forest as a continuous bulk medium with nearly perfect optical absorption and anisotropic thermal conductivity. This is appropriate if the illuminated spot is large enough to cover many CNTs, which is the case in typical heat trap experiments where hundreds to thousands of CNTs are covered by the illuminating beam spot. In this context, the many individual photon and electron emission and reabsorption events within the bulk of the CNT forest lead to an effective photon emission (incandescence) and electron emission (thermionic emission) from the surface of the forest—now represented by a continuous bulk—as seen in the “Methods” section in Supplemental Material [25]. Finally, we note that thermal conductivity depends on temperature [26]. Importantly, the temperature dependence of thermal conductivity may itself be affected by dimensionality: whereas in three-dimensional (3D) crystals thermal conductivity may peak at a temperature of a few tens of kelvins and then decline with a characteristic $\sim T^{-1}$ behavior due to Umklapp phonon scattering, in two-dimensional (2D) and 1D materials such as graphene ribbons and carbon nanotubes, the peak may happen

at hundreds of kelvins [27–31]. Therefore, for applications at room temperature and above, the role of the temperature dependence of thermal conductivity is expected to be highly pronounced in these materials.

Our model is founded on two critical observations:

(1) Heat flow along a given direction in a material is affected by the thermal conductivity not only in that direction but also in the transverse directions;

(2) A decrease in thermal conductivity with temperature leads to a snowballing rise in local temperature.

We use the model (see the “Methods” section in Supplemental Material [25] for details and past literature on solving the heat equation [32–40]) to calculate the temperature distribution in a material illuminated by a Gaussian optical beam with a spot diameter of 100 μm , and compare three cases: (1) 3D isotropic; (2) 2D anisotropic, where thermal conductivity along the depth is 100 times lower than along the surface directions; and (3) 1D anisotropic, where thermal conductivities along the depth and one of the surface directions are 100 times lower than along the other surface direction. These are meant to conceptually represent various physical situations (a bulk, a layered structure such as multilayer graphene, and an array of nanotubes/nanowires such as a CNT forest). To allow for a fair comparison, in each case, we consider three behaviors for thermal conductivity, all starting with a value of 100 W/mK at room temperature: (1) constant, (2) decreasing with temperature as $\sim T^{-1}$ (due to Umklapp phonon scattering [41]), and (3) decreasing with temperature primarily as $\sim T^{-2}$ at high temperatures (due to higher-order scattering) as, for example, suggested for CNTs [30]. The complete functional forms of the temperature dependences we have used are given in Supplemental Material [25]. For brevity, throughout the paper we refer to those as constant, T^{-1} , and T^{-2} , respectively. Note that the numerical values of the results presented below depend directly on our specific choice for the functional form of thermal conductivity; therefore, we put no emphasis on the exact values of temperature gradient or other quantities we report, but our goal is to show a qualitative comparison among the different cases of anisotropy and temperature dependence of thermal conductivity.

III. RESULTS AND DISCUSSION

Figure 3 shows our central result: the temperature distribution on the illuminated surface. In the first row, a significantly higher peak temperature of 3000 K is achieved for the 1D case (versus 1411 K for the 2D case and 421 K for the 3D case), with a maximum temperature gradient along the longitudinal, high-conductivity direction (y axis) of 20.4 K/ μm (versus 14.8 K/ μm for the 2D case and 1.7 K/ μm for the 3D case). In the 1D case, not only is the temperature confined along the transverse, low-conductivity direction (x axis) but it is also highly confined along the high-conductivity axis, in sharp contrast to the 3D and 2D cases. Limiting thermal conductivity in transverse directions thus has a decisive impact on temperature distribution along the high-conductivity axis as well. This may be viewed as a consequence of the fact that heat takes infinitely many paths in all directions in going from one point to another, and thus the different directions cannot be viewed as independent. This can be directly appreciated

based on Eq. (6) in Supplemental Material [25], where it is seen that the entire spatial distribution of the so-called linear temperature (an intermediate variable in the calculation of true temperature) is inversely proportional to $(\alpha\beta\gamma^2)^{1/4}$, where α , β , and γ are the anisotropy factors of thermal conductivity associated with the three directions. In other words, the temperature profile in any direction is affected by conductivity in all three directions.

Comparing the three panels in the third column of Fig. 3, we note that the temperature localization described above is strongly amplified if thermal conductivity is a decreasing function of temperature, the effect being more severe the steeper the decrease. We interpret this as a runaway effect due to a positive feedback: a rise in temperature leads to a corresponding drop in local thermal conductivity, which in turn leads to further increase in local temperature and so on. This is as if, at high temperatures, the increase in the population of high-momentum phonons leads to a phonon traffic jam that restricts heat conduction (through Umklapp scattering). The value of total input optical power for each row of Fig. 3 has been chosen so as to obtain the same peak temperature of 3000 K for the 1D case. Note that the required power has decreased by over 50 times, from 1.55 to 0.75 and then 0.028 W, by going from a constant thermal conductivity to one behaving as T^{-1} and then T^{-2} . The effect of anisotropy is also most pronounced in the latter case: whereas a modest input optical power of 28 mW enables the 1D T^{-2} material to reach ~ 3000 K and a maximum temperature gradient of 282.9 K/ μm , it has essentially negligible effect on the 2D and 3D cases. Similarly, this amount of input power would not lead to significant temperature increase even in the 1D case if the thermal conductivity did not decrease rapidly with temperature. We point out that, while the dimensionality and the temperature dependence of thermal conductivity each play a decisive role in heat flow and the resulting temperature profile, their effects are ultimately mixed and the former can exacerbate the latter, as illustrated by the extremely strong and confined heating seen in Fig. 3(k).

Figures 3(k) and 3(l) also reveal the striking feature of a hot spot that is significantly smaller than the illuminating beam spot: whereas the optical beam has an e^{-2} diameter of 100 μm , the full width at half maximum (FWHM) of the resulting temperature profile is only 12.52 μm along the y axis. Also, note that even stronger confinement and higher temperature gradients result for smaller illuminations spots. For example, for a 1- μm -diameter beam, the 1D T^{-2} -conductivity material would yield a staggering maximum temperature gradient of 13470 K/ μm with 777 μW of input power, with a peak temperature of 2987 K and an extremely confined temperature profile with a FWHM of 258 nm. (It should be noted that, at extremely high temperature gradients, a microscopic treatment of the temperature distribution on the individual CNTs involved may be necessary and Fourier’s law may not apply [42], and that even the correct definition of temperature at that scale in nonequilibrium requires care [43], so the results in that regime are of qualitative value, rather than being exact predictions.)

It would also be instructive to examine the spatial distribution of thermal conductivity under localized heating. Since thermal conductivity is a tensor, instead of plotting its various

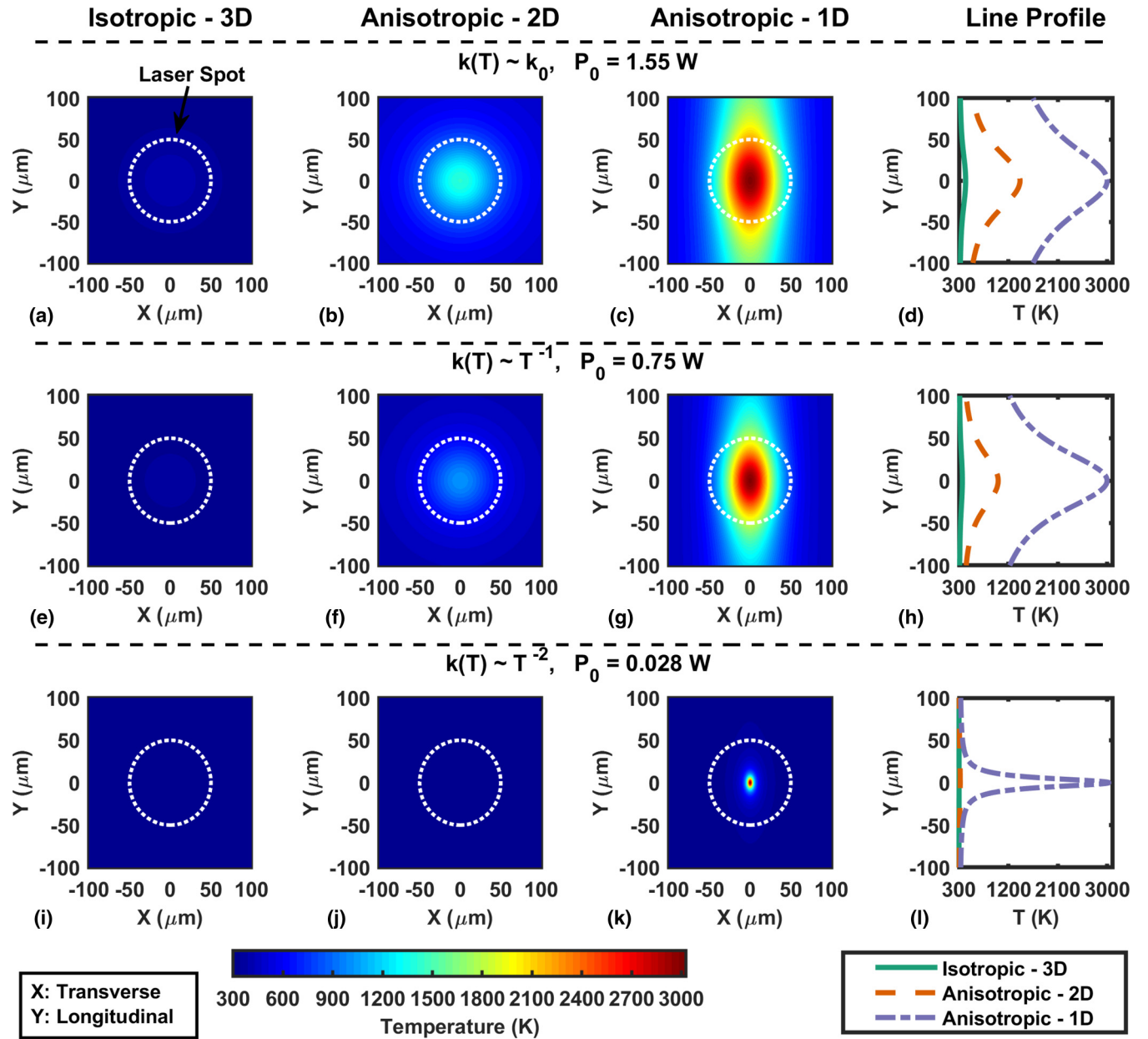


FIG. 3. Calculated temperature distribution on the illuminated surface. The first three columns from the left are for the 3D, 2D, and 1D cases, respectively, and the fourth column shows the cross section of the profile along the y axis (direction of high thermal conductivity) for all three cases. The different rows correspond to the different temperature dependences of thermal conductivity (constant, T^{-1} , and T^{-2} , respectively). For each such temperature dependence, the value of the input optical power has been chosen so as to result in a peak temperature of 3000 K for the 1D case. The dashed circle represents the illuminating beam spot, which has an e^{-2} diameter of 100 μm .

components separately, and inspired by the mixing of the three components as discussed before, we have defined an effective thermal conductivity as $(\alpha\beta\gamma^2)^{1/4} k(T)$ in order to simultaneously capture the effects of anisotropy and temperature dependence. Figure 4 shows the spatial distribution of this effective thermal conductivity for all the cases of temperature distribution depicted in Fig. 3. In the first row, the effective conductivity is constant throughout space, but is reduced progressively when going from 3D to 2D to 1D. In the second row, the T^{-1} behavior leads to the creation of an effectively thermally isolated area in the middle of the

conductor's surface, but the effect is negligible in the 3D case and moderate in the 2D case; it is much stronger in the 1D case. This local thermal isolation becomes much more pronounced with the T^{-2} behavior as shown in the third row.

Figure 5 illustrates the peak temperature and the FWHM (along the high-conductivity axis) of the temperature profile versus input optical power. We see that the 1D case reaches high temperatures at much lower input powers than the 2D and 3D cases. For constant thermal conductivity, the temperature rises linearly (until incandescence and thermionic emission losses become significant—not shown). For a decreasing

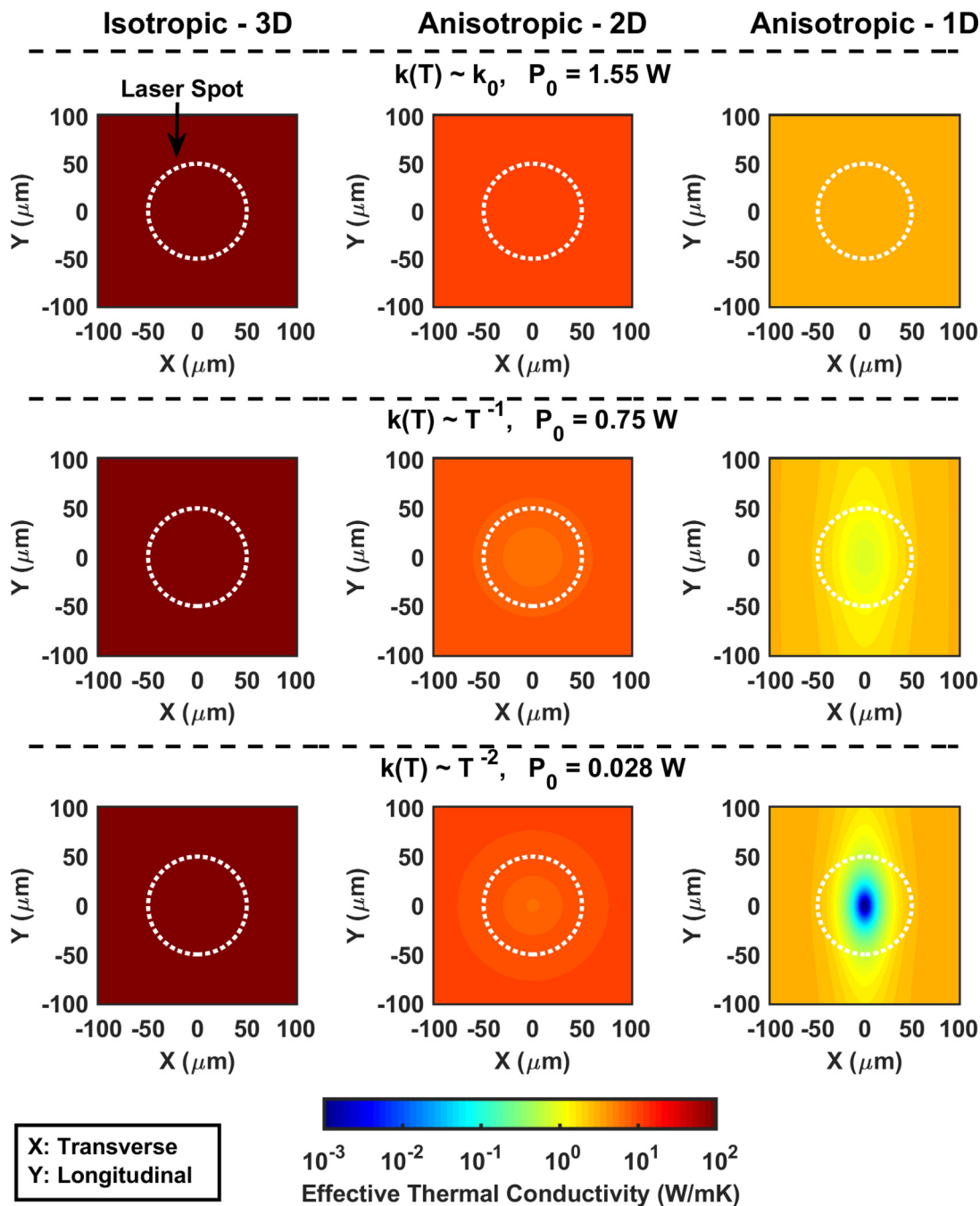


FIG. 4. Calculated effective thermal conductivity, $(\alpha\beta\gamma^2)^{1/4} k(T)$, on the illuminated surface corresponding to the various cases of temperature distribution shown in Fig. 3.

thermal conductivity, the temperature grows nonlinearly, with the effect being significantly more pronounced for the T^{-2} dependence. This effect takes over at much lower input powers for the 1D case, where heat transfer is severely constricted as discussed before.

We define a heating efficiency as the portion of incident power that is converted to thermionic emission and incandescence (as opposed to dissipated through conduction). While, assuming a work function of 2.5 eV, the heating efficiency for 3D T^{-2} conductivity is only 1.95% at 3000 K, it reaches 34.98% for 1D T^{-2} conductivity. The trends in peak temperature and temperature spread as a function of

illuminated spot size, relative strength of thermionic emission and incandescence, heating efficiency, and results based on a temperature-dependent thermal conductivity measured for actual CNTs are presented in Supplemental Material [25]. In particular, the model predicts that for a given optical intensity a higher temperature is achieved with an increase in the size of the illuminating spot (see Fig. S2 in Supplemental Material [25]). This comes from the fact that intensity depends on the inverse square of the spot diameter, whereas the primary heat conduction cross-sectional area (which is perpendicular to the nanotubes axis) is linearly proportional to the spot diameter, meaning that heat conduction along the nanotubes

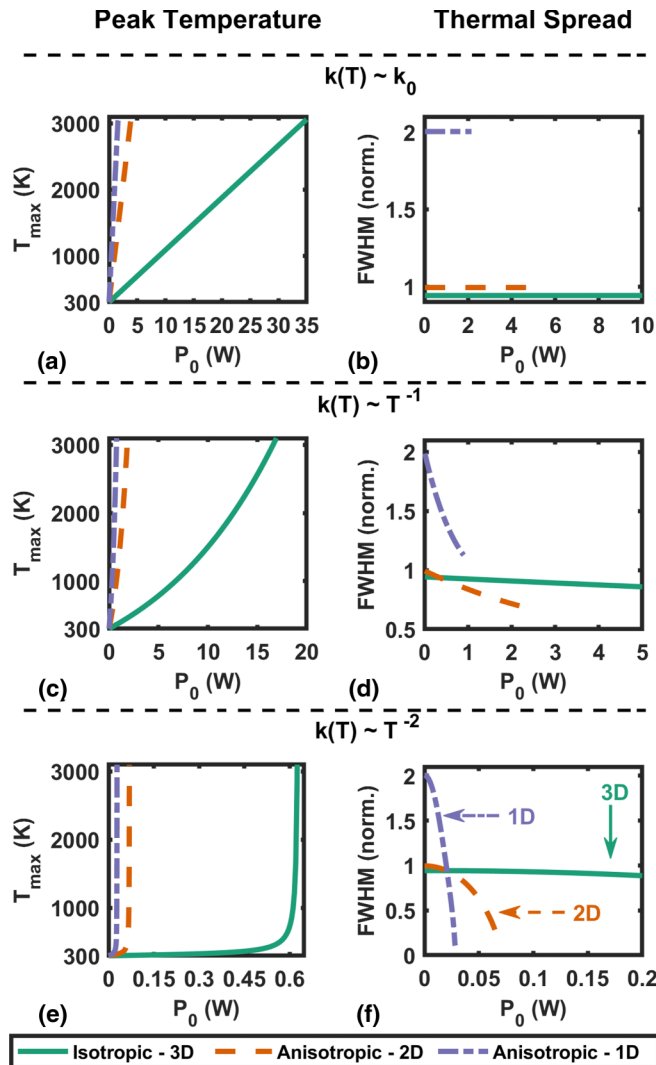


FIG. 5. Trends with input power. Peak temperature (a, c, e) and thermal spread normalized to the incident beam radius (b, d, f) for (a, b) constant, (c, d) T^{-1} , and (e, f) T^{-2} thermal conductivity behaviors, as a function of the input power. The thermal spread is shown for the y direction, which is along the nanotubes.

becomes relatively more difficult for wider spots. At the nano and meso scales, this may be viewed as follows: The radiation from each nanotube is partially reabsorbed by the adjacent nanotubes, such that each would absorb a higher effective power than if it were isolated. Therefore, starting from one nanotube and gradually placing additional ones adjacent to it, an increase in the temperature of the illuminated spot is expected. This may partially explain why experiments on optically heated individual CNTs [16,17] have yielded much lower temperature levels compared to those on CNT forests [9].

Finally, we note that anisotropic thermal conductivity is not limited to 1D systems. For instance, black phosphorous also exhibits anisotropic thermal conductivity even within its basal plane [44]; its thermal conductivity also shows a peak at

around 100 K and decays well past room temperature [45]. Therefore, the approach and model described here are not limited to CNTs. We also note that we have assumed the incandescence to follow Planck's law. While CNT forests are near-ideal black materials as mentioned before, a heat trap may represent a nonequilibrium condition. Among other effects, the electronic and lattice temperatures may be different, as has also been observed in graphite and van der Waals heterostructures [46–48], and deviations from the blackbody radiation law are possible. However, prior works have shown good agreement with the blackbody radiation law for CNTs [49,50]. Our ongoing work nonetheless involves incandescence spectroscopy over a broad range to elucidate possible deviations from Planck's law. We also point out that extremely large temperature gradients have also been observed in other low-dimensional systems such as silicon and aluminum wires with submicron diameters [51,52], which further suggests that such heat localization may be a general property arising from low dimensionality, rather than being limited to carbon nanotubes. We should also emphasize that an overall low thermal conductivity would also obviously lead to some degree of heat localization. (Given the porous and defective nature of the CNT forest and the internanotube entanglements thereof, it is expected to have a lower thermal conductivity than pristine nanotubes.) Other published mechanisms such as Anderson localization or discrete breathers [53,54] could also play a role in limiting heat flow. We thus do not claim that our proposed mechanism is a necessary condition for the heat trap effect, but that it is a sufficient one for it. It is also worth noting that, while we considered optical illumination for heating, similar localization effects might take place even if the input power is delivered through other means such as Joule heating [55–57].

IV. SUMMARY

In summary, we have demonstrated that material dimensionality/anisotropy, combined with the fact that thermal conductivity decreases with temperature, can result in strong localization of heat with extremely high temperature gradients in a direction where thermal conductivity is intrinsically high. This represents a mechanism for controlling heat flow in conductors, with significant implications: It means that one can maintain a high temperature difference between two points that are electrically connected, or create localized electron sources using low excitation powers. These could lead to breakthroughs in thermoelectricity and thermionics for energy conversion and a variety of other applications.

ACKNOWLEDGMENTS

We acknowledge financial support from the Natural Sciences and Engineering Research Council of Canada (Grants No. SPG-P 478867, No. RGPIN-2017-04608, and No. RGPAS-2017-507958), the Canada Foundation for Innovation, the British Columbia Knowledge Development Fund, and the Peter Wall Institute for Advanced Studies. This research was undertaken thanks in part to funding from the Canada First Research Excellence Fund, Quantum Materials and Future Technologies Program.

- [1] H. Pfau, S. Hartmann, U. Stockert, P. Sun, S. Lausberg, M. Brando, S. Friedemann, C. Krellner, C. Geibel, S. Wirth, S. Kirchner, E. Abrahams, Q. Si, and F. Steglich, *Nature (London)* **484**, 493 (2012).
- [2] S. Lee, K. Hippalgaonkar, F. Yang, J. Hong, C. Ko, J. Suh, K. Liu, K. Wang, J. J. Urban, X. Zhang, C. Dames, S. A. Hartnoll, O. Delaire, and J. Wu, *Science* **355**, 371 (2017).
- [3] T. Takabatake, K. Suekuni, T. Nakayama, and E. Kaneshita, *Rev. Mod. Phys.* **86**, 669 (2014).
- [4] G. S. Nolas, D. T. Morelli, and T. M. Tritt, *Annu. Rev. Mater. Sci.* **29**, 89 (1999).
- [5] A. Balandin and K. L. Wang, *Phys. Rev. B* **58**, 1544 (1998).
- [6] A. Balandin and K. L. Wang, *J. Appl. Phys.* **84**, 6149 (1998).
- [7] A. Khitun, A. Balandin, and K. L. Wang, *Superlatt. and Microstruct.* **26**, 181 (1999).
- [8] Y. D. Kim, H. Kim, Y. Cho, J. H. Ryoo, C.-H. Park, P. Kim, Y. S. Kim, S. Lee, Y. Li, S.-N. Park, Y. S. Yoo, D. Yoon, V. E. Dorgan, E. Pop, T. F. Heinz, J. Hone, S.-H. Chun, H. Cheong, S. W. Lee, M.-H. Bae, and Y. D. Park, *Nat. Nanotechnol.* **10**, 676 (2015).
- [9] P. Yaghoobi, M. V. Moghaddam, and A. Nojeh, *Solid State Commun.* **151**, 1105 (2011).
- [10] M. Chang, M. Vahdani Moghaddam, A. Khoshaman, M. S. Mohamed Ali, M. Dahmardeh, K. Takahata, and A. Nojeh, *Proceedings of the 57th International Conference on Electron, Ion, and Photon Beam Technology and Nanofabrication* (American Vacuum Society, 2013), p. 11-08.
- [11] H. D. E. Fan, G. A. Sawatzky, J. F. Young, and A. Nojeh, *Proceedings of the 30th International Vacuum Nanoelectronics Conference, Proc. No. NMC-CI* (IEEE, Piscataway, NJ, 2017), p. 44.
- [12] Y. Wei, K. Jiang, X. Feng, P. Liu, L. Liu, and S. Fan, *Phys. Rev. B* **76**, 045423 (2007).
- [13] M. Vahdani Moghaddam, P. Yaghoobi, and A. Nojeh, *Appl. Phys. Lett.* **101**, 253110 (2012).
- [14] P. Yaghoobi, M. Vahdani Moghaddam, and A. Nojeh, *AIP Adv.* **2**, 042139 (2012).
- [15] M. Vahdani Moghaddam, P. Yaghoobi, G. A. Sawatzky, and A. Nojeh, *ACS Nano* **9**, 4064 (2015).
- [16] I.-K. Hsu, M. T. Pettes, A. Bushmaker, M. Aykol, L. Shi, and S. B. Cronin, *Nano Lett.* **9**, 590 (2009).
- [17] D. Rossouw, M. Bugnet, and G. A. Botton, *Phys. Rev. B* **87**, 125403 (2013).
- [18] K. Mizuno, J. Ishii, H. Kishida, Y. Hayamizu, S. Yasuda, D. N. Futaba, M. Yumura, and K. Hata, *Proc. Natl. Acad. Sci. USA* **106**, 6044 (2009).
- [19] R. Fainchtein, D. M. Brown, K. M. Siegrist, A. H. Monica, E. Hwang, S. D. Milner, and C. C. Davis, *Phys. Rev. B* **85**, 125432 (2012).
- [20] Z.-P. Yang, L. Ci, J. A. Bur, S.-Y. Lin, and P. M. Ajayan, *Nano Lett.* **8**, 446 (2008).
- [21] J. Che, T. Çağın, and William A Goddard III, *Nanotechnology* **11**, 65 (2000).
- [22] I. Ivanov, A. Puzdov, G. Eres, H. Wang, Z. Pan, H. Cui, R. Jin, J. Howe, and D. B. Geohegan, *Appl. Phys. Lett.* **89**, 223110 (2006).
- [23] M. B. Jakubinek, M. A. White, G. Li, C. Jayasinghe, W. Cho, M. J. Schulz, and V. Shanov, *Carbon* **48**, 3947 (2010).
- [24] M. Isaiev, O. Didukh, T. Nychporuk, V. Timoshenko, and V. Lysenko, *Appl. Phys. Lett.* **110**, 011908 (2017).
- [25] See Supplemental Material at <http://link.aps.org/supplemental/10.1103/PhysRevB.98.155422> for methods, the trends in peak temperature and temperature spread as a function of illuminated spot size, relative strength of thermionic emission and incandescence, heating efficiency, and results based on a temperature-dependent thermal conductivity measured for actual carbon nanotubes.
- [26] C. Y. Ho, R. W. Powell, and P. E. Liley, *J. Phys. Chem. Ref. Data* **1**, 279 (1972).
- [27] A. Cepellotti, G. Fugallo, L. Paulatto, M. Lazzeri, F. Mauri, and N. Marzari, *Nat. Commun.* **6**, 6400 (2015).
- [28] S. Berber, Y.-K. Kwon, and D. Tománek, *Phys. Rev. Lett.* **84**, 4613 (2000).
- [29] M. A. Osman and D. Srivastava, *Nanotechnology* **12**, 21 (2001).
- [30] E. Pop, D. Mann, Q. Wang, K. Goodson, and H. Dai, *Nano Lett.* **6**, 96 (2006).
- [31] G. Zhang and B. Li, *J. Chem. Phys.* **123**, 114714 (2005).
- [32] Y.-F. Lu, *J. Appl. Phys.* **72**, 4893 (1992).
- [33] J. F. Ready, *J. Appl. Phys.* **36**, 462 (1965).
- [34] H. Grönbeck and M. Reichling, *J. Appl. Phys.* **78**, 6408 (1995).
- [35] B. S. Yilbas and N. Al-Aqeeli, *Opt. Laser Technol.* **41**, 132 (2009).
- [36] Y. Gurevich, N. Filonenko, and N. Salansky, *Appl. Phys. Lett.* **64**, 3216 (1994).
- [37] M. Lax, *Appl. Phys. Lett.* **33**, 786 (1978).
- [38] Y.-F. Lu, *Appl. Phys. Lett.* **61**, 2482 (1992).
- [39] Y. I. Nissim, A. Lietoila, R. B. Gold, and J. F. Gibbons, *J. Appl. Phys.* **51**, 274 (1980).
- [40] J. E. Moody and R. H. Hendel, *J. Appl. Phys.* **53**, 4364 (1982).
- [41] E. Pop, D. Mann, J. Cao, Q. Wang, K. Goodson, and H. Dai, *Phys. Rev. Lett.* **95**, 155505 (2005).
- [42] C. W. Chang, D. Okawa, H. Garcia, A. Majumdar, and A. Zettl, *Phys. Rev. Lett.* **101**, 075903 (2008).
- [43] D. G. Cahill, W. K. Ford, K. E. Goodson, G. D. Mahan, A. Majumdar, H. J. Maris, R. Merlin, and S. R. Phillpot, *J. Appl. Phys.* **93**, 793 (2003).
- [44] J. Zhu, H. Park, J.-Y. Chen, X. Gu, H. Zhang, S. Karthikeyan, N. Wendel, S. A. Campbell, M. Dawber, X. Du, M. Li, J.-P. Wang, R. Yang, and X. Wang, *Adv. Electron. Mater.* **2**, 1600040 (2016).
- [45] B. Sun, X. Gu, Q. Zeng, X. Huang, Y. Yan, Z. Liu, R. Yang, and Y. K. Koh, *Adv. Mater.* **29**, 1603297 (2017).
- [46] Q. Ma, T. I. Andersen, N. L. Nair, N. M. Gabor, M. Massicotte, C. H. Lui, A. F. Young, W. Fang, K. Watanabe, T. Taniguchi, J. Kong, N. Gedik, F. H. L. Koppens, and P. Jarillo-Herrero, *Nat. Phys.* **12**, 455 (2016).
- [47] M. Massicotte, P. Schmidt, F. Vialla, K. Watanabe, T. Taniguchi, K. J. Tielrooij, and F. H. L. Koppens, *Nat. Commun.* **7**, 12174 (2016).
- [48] S. Tan, A. Argondizzo, C. Wang, X. Cui, and H. Petek, *Phys. Rev. X* **7**, 011004 (2017).
- [49] P. Li, K. Jiang, M. Liu, Q. Li, and S. Fan, *Appl. Phys. Lett.* **82**, 1763 (2003).
- [50] Y. Fan, S. B. Singer, R. Bergstrom, and B. C. Regan, *Phys. Rev. Lett.* **102**, 187402 (2009).
- [51] G. Bakan, N. Khan, A. Cywar, K. Cil, M. Akbulut, A. Gokirmak, and H. Silva, *J. Mat. Res.* **26**, 1061 (2011).

- [52] M. Mecklenburg, W. A. Hubbard, E. R. White, R. Dhall, S. B. Cronin, S. Aloni, and B. C. Regan, *Science* **347**, 629 (2015).
- [53] H. Hu, A. Strybulevych, J. H. Page, S. E. Skipetrov, and B. A. van Tiggelen, *Nat. Phys.* **4**, 945 (2008).
- [54] S. Flach and A. V. Gorbach, *Phys. Rep.* **467**, 1 (2008).
- [55] S. T. Purcell, P. Vincent, C. Journet, and V. Thien Binh, *Phys. Rev. Lett.* **88**, 105502 (2002).
- [56] P. Vincent, S. T. Purcell, C. Journet, and V. T. Binh, *Phys. Rev. B* **66**, 075406 (2002).
- [57] X. Wei, S. Wang, Q. Chen, and L. Peng, *Sci. Rep.* **4**, 5102 (2014).